

Dislocation-mediated flux creep in $\text{Bi}_2\text{Sr}_2\text{CaCu}_2\text{O}_{8+\delta}$

C. J. van der Beek and P. H. Kes*

Kamerlingh Onnes Laboratorium der Rijksuniversiteit Leiden, P. O. Box 9506, 2300 RA Leiden, The Netherlands

(Received 8 October 1990; revised manuscript received 22 April 1991)

We have investigated the possible role of two-dimensional vortex-lattice defects in thermally assisted flux flow for the very anisotropic high-temperature superconductor $\text{Bi}_2\text{Sr}_2\text{CaCu}_2\text{O}_{8+\delta}$ (Bi-Sr-Ca-Cu-O). At low current densities, this mechanism, which we shall refer to as plastic flux creep, is expected to prevail over creep of elastically correlated flux bundles, or elastic creep. It is assumed that vortices are pinned by oxygen vacancies, for which the elementary interaction is obtained. Measurements of the ac susceptibility in an applied dc field, $B_{c1} < \mu_0 H < 0.2B_{c2}$, carried out using a sufficiently low driving-field amplitude, were performed on a Bi-Sr-Ca-Cu-O single-crystalline sample. It is shown that under the above assumptions the experimental data may be consistently interpreted. The field dependence of the activation barrier is explained. Furthermore, the irreversibility line is reproduced, as well as the shape of the ac-susceptibility transition. Deviations from the plastic-flux-creep model can be qualitatively understood using a criterion describing the crossover to elastic flux creep.

I. INTRODUCTION

It is well established that thermal fluctuations and flux creep play an important role in high-temperature superconductors (HTS's), even at temperatures well below T_c . These processes are reflected by such experimental results as a strongly time-dependent value of the dc magnetization,¹ an extreme broadening of the resistive transition,^{2,3} and the strong frequency and field dependence of the ac-susceptibility transition.⁴⁻⁶ Different authors have interpreted these results in terms of melting of the Abrikosov flux lattice,⁷⁻¹⁰ as a transition from vortex glass to vortex liquid,¹¹ or as a thermally assisted flux flow (TAFF).¹² In either case the interaction between vortices and pinning centers is expected to play a role.¹³ Vortices experience a certain pinning potential U that should be overcome on the time scale set by experiment in order for flux motion to be observed. In TAFF (Ref. 12) it was assumed that this quantity is equal to the pinning energy U_c as this follows from the theory of collective flux pinning,¹⁴ i.e., independent of driving force. Recently, however, it was shown theoretically¹⁵ that when the vortex lattice (VL) is pinned (vortex glass state), U should scale with the current density j (proportional to the driving force) as

$$U = U_c \left(\frac{j_c}{j} \right)^y. \quad (1)$$

The exponent y depends on the dimensionalities of the flux bundle and of the translational vector describing its position. U_c is the potential barrier in collective pinning theory and is attained when j equals the critical current density j_c . In the case of three-dimensional collective pinning (3DCP), this U_c depends on the pinning mechanism, characterized by the pinning strength γ and range r_f (see below). The origin of the pinning in HTS's is still the subject of considerable discussion, the main candi-

dates being intrinsic pinning,¹⁶ pinning by extended defects such as intergrowths,² or second phases,¹⁷ or by point defects, such as oxygen vacancies.

The theory of collective flux creep as developed by Feigel'man *et al.*¹⁵ only considers the elastic deformation of the vortex lattice by defects in the crystal lattice. Their main result [Eq. (1)] clearly imposes a limit on any flux-transfer mechanism based on elastic flux creep. At low current densities the activation barrier will grow to such an extent that any observable flux motion on experimental time scales is inhibited. Nevertheless, as will be shown below, an ac-susceptibility experiment on Bi-Sr-Ca-Cu-O carried out using a low driving field, i.e., at low j , shows significant frequency dependence of the diamagnetic transition (see also Ref. 6). This is indicative of flux motion over macroscopic distances within the driving-field cycle. Therefore, an alternative to elastic creep of flux bundles needs to be considered.

Experiments on $a\text{-Nb}_x\text{Ge}$ and $a\text{-Mo}_x\text{Si}$ thin films¹⁸ have shown that even in materials with weak pinning the VL becomes unstable to the formation of plastic deformations when high stresses are applied. The positional order of the vortices is reduced, resulting in the well-known peak effect in the critical current. In three dimensions it is energetically much more favorable for the VL to contain numerous screw dislocations, resulting in a highly disordered state, far from what might be expected from three-dimensional collective pinning theory.¹⁹ Evidence for the domination of flux flow in two dimensions (2D) by the plastic deformation of the VL has been brought forward in Ref. 20. In the present paper we shall therefore compare results of magnetic measurements on a Bi-Sr-Ca-Cu-O single crystal with a model based on the presence of dislocations in the VL.

The idea to be pursued is that when a static magnetic field is applied to a type-II superconductor at a finite temperature, the magnetization decays with time according

to elastic creep theory, starting from the critical state. As the magnetization and corresponding current density in the sample decrease, the activation barrier $U(j)$ for elastic flux creep increases, following Eq. (1). Eventually, the current density will become so small that $U(j)$ will increase above the relevant energy for motion of VL dislocations.

We now summarize the contents of the paper. In Sec. II the model of plastic flux creep in a very anisotropic superconductor is outlined. Because of the extreme anisotropy of the material, it is more appropriate to treat the mixed state in Bi-Sr-Ca-Cu-O as an array of superposed 2D vortex lattices, situated in the (superconducting) CuO_2 double layers. Next, we consider the plastic deformation of these 2D vortex lattices, i.e., the introduction of edge-dislocation pairs. Associated are two characteristic energies: the dislocation nucleation energy, which depends on the VL shear modulus c_{66} , and the pinning energy. In the following we will assume pinning to occur by oxygen vacancies in the CuO_2 double layers, for which the elementary pinning force will be derived. Once these quantities are established, we recognize that motion of a small dislocation pair, unlike that of a fluxon bundle, involves only fixed length scales and may be thus described as diffusion of a particle. For the associated flux transport, TAFF theory¹² is appropriate. This will be briefly reviewed for the application to ac-susceptibility experiments. In that case diffusion is driven by the periodic variation in time of the applied field at the sample surface. The resulting flux profile decays exponentially over a characteristic length λ_{ac} . In Sec. III measurements on a Bi-Sr-Ca-Cu-O single crystal are presented and compared with theory. The results are discussed in Sec. IV. Throughout the paper we will only consider the low-field case $b \equiv B/B_{c2} < 0.2$ of isolated vortices.

II. THEORY

A. Dimensionality of the Bi-Sr-Ca-Cu-O compound

A consequence of the crystal structure of the HTS's, which features weakly coupled parallel CuO_2 layers, is the often huge anisotropy in the effective mass of the charge carriers. For Bi-Sr-Ca-Cu-O this amounts to a factor $\Gamma \equiv m_c/m \approx 3000$.²¹ Here m and m_c are the carrier effective masses parallel and perpendicular to the CuO_2 planes, respectively. Since the anisotropy factor Γ enters in the expression for the tilt modulus of the VL,¹⁰ $\tilde{c}_{44} \approx c_{44}/\Gamma$, this quantity is reduced, to a remarkable extent, well below the value of the shear modulus $c_{66} \approx (B_c^2/4\mu_0)b$ (B_c is the thermodynamic critical field). This reflects the instability of the vortices to segmentation along the c direction. Indeed, the longitudinal characteristic dimension L_c of a correlated volume of the VL, as this follows from the theory of collective flux pinning,¹⁴ was calculated to be of the order of the thickness d of a CuO_2 double layer.²² Below a crossover field $B_{2D} = \Phi_0/\Gamma d^2$, magnetic coupling between vortices in adjacent CuO_2 layers becomes important ($\Phi_0 = h/2e$ is the flux quantum). For Bi-Sr-Ca-Cu-O this amounts to a

field $B_{2D} \approx 0.3$ T demarcating a low-field regime where the VL is expected to display a three-dimensional character^{22–24} and a high-field region where a description in terms of weakly coupled two-dimensional superconducting layers seems justified.²⁵ Below, we will treat Bi-Sr-Ca-Cu-O as a 2D layered superconductor, with a layer thickness $d \approx 1.2–1.5$ nm, corresponding to the spacing between CuO_2 planes, or half the size of the unit cell. The vortex structure in the mixed state then consists of independent arrays of 2D vortices within the CuO_2 layers. Between these layers the order parameter is exponentially small.²⁶

B. Edge dislocations in the vortex lattice

Models for thermally activated motion of defects in the VL were developed by Vinokur, Kes, and Koshelev²² and by Feigel'man, Geshkenbein, and Larkin.²³ In a 2D vortex lattice, the relevant defects are pairs of edge dislocations, corresponding to extra or missing rows of vortices. Once such a dislocation pair has been nucleated, a vortex row constrained between these can move relatively easily through the vortex lattice and transport flux through the superconductor. Small pairs where the distance between dislocations approximately equals the vortex spacing, $a_0 \approx \sqrt{(\Phi_0/B)}$, are expected to be the main contributors to flux creep, because their nucleation energy U_e is lowest. For such pairs, which can be seen as VL vacancies or interstitials, this amounts to

$$U_e \approx \frac{1}{\pi} c_{66} d a_0^2 = \frac{\Phi_0^2 d}{4\pi^2 \mu_0 \lambda^2}, \quad (2)$$

where λ is the effective penetration depth. Here interactions between pairs are neglected. If we take $\lambda \approx 290$ nm,^{27,28} this nucleation energy is approximately 100 K. Note that U_e is almost constant in the temperature region $T < 50$ K, to be considered below. In the absence of pinning, the diffusivity of the dislocations is determined by their (thermally induced) concentration $n_v a_0^2$, which will be proportional to $\exp(-U_e/k_B T)$.

C. Pinning of small edge-dislocation pairs

The second important energy relevant to the problem is that associated with the pinning of a VL interstitial (or vacancy). The presence of pinning not only results in a small, approximately constant, residual concentration of VL defects, i.e., disorder even at zero temperature, but also constitutes an impedance to interstitial motion through the VL. In order to estimate the associated energy barrier, the strength of the pinning potential must be evaluated. The pinning potential experienced by an interstitial is that of a single vortex. This is written as the product of the pinning force per vortex and the pinning range:

$$U_v = F_v r_f. \quad (3)$$

Since we are dealing with the low-field limit, the pinning range r_f will be taken to be the Ginzburg-Landau coher-

ence length $\xi(T)$.²⁹ Because of the perovskite-related nature of the materials, important candidates for the pinning mechanism in HTS's in general are oxygen vacancies in the CuO_2 layers. Oxygen vacancies can be described as small voids with diameter D_v , which interact with a vortex core mainly through quasiparticle scattering. It was shown by Thuneberg, Kurkijärvi, and Rainer,³⁰ that the effective defect volume is enhanced with respect to D_v^3 by a factor ξ_0/D_v . It therefore equals the product of the defect scattering cross section $\sigma_{\text{tr}} = \pi D_v^2/4$ and the BCS coherence length ξ_0 . The pinning potential as a function of distance from defect to vortex core for the case of weak scattering was calculated in Ref. 30. Taking the derivative yields the elementary interaction

$$f(r) \approx 2.3 f_p \frac{r}{r_0} \exp\left[-\frac{r^2}{r_0^2}\right], \quad (4a)$$

$$f_p \approx \frac{12.0}{(1+t)^4} g(\rho_D) \frac{B_c^2}{\mu_0 \xi} \sigma_{\text{tr}} \xi_0. \quad (4b)$$

$B_c^2/2\mu_0$ is the condensation energy, r is the distance from the center of the oxygen vacancy, $r_0 \approx 0.81\xi(T)$, and $t \equiv T/T_c$. The function $g(\rho_D)$ is given by $0.882\chi'(\rho_D)/\chi(\rho_D)$, where $\chi(\rho_D)$ is the Gor'kov function and ρ_D the dirt parameter ξ_0/l . In the pure limit ($l > \xi_0$), $g(\rho_D) \approx 0.85$. Substituting the parameter values $B_c(0) \approx 0.3$ T, $\xi_0 = 1.35\xi(0)$, and $D_v \approx 0.29$ nm, the *maximum* strength of the elementary pinning force f_p was evaluated at 6.5×10^{-14} N at low temperatures. It is interesting to note that f_p is not influenced by the small coherence length: f_p is larger than the same quantity in conventional superconductors only because of the larger condensation energy.

The validity of Eq. (4b) for the elementary interaction is limited by the oxygen vacancy density n_{\square} . Note that n_{\square} is the areal density of pinning centers per CuO_2 double layer. When it increases it is expected that f_p is reduced as a result of the effect of background scattering from many other oxygen vacancies.³⁰ The averaging effect becomes unimportant when $n_{\square}\xi D_v < 1$. We shall see below that this condition is satisfied, allowing us to neglect this effect.

From the elementary interaction the macroscopic pinning force per vortex is evaluated using the collective pinning concept $F_v = \sqrt{n_{\square}\pi\xi^2\langle f^2 \rangle} \equiv \gamma^{1/2}$. The averaging $\langle f^2 \rangle$ should be taken over the vortex core. Inserting the result $0.89f_p^2$ in the expression for F_v , the pinning energy per vortex becomes

$$U_v \approx \left[\pi n_{\square} \xi^2 f_p^2 \right]^{1/2} r_f \\ \approx \frac{21}{(1+t)^4} n_{\square}^{1/2} g(\rho_D) \left[\frac{B_c^2}{\mu_0 \xi} \sigma_{\text{tr}} \xi_0 \right] \xi^2. \quad (5)$$

The pinning strength can be characterized by the value of a dimensionless parameter $\alpha \equiv (\mu_0 U_v / B_c^2 \xi^2 d)^2$.²² A value of α much less than 1 implies collective pinning of the VL; a value $\alpha \lesssim 1$ means that although the interaction of

the pinning centers with a vortex is still collective, vortices are now pinned independently. Note that U_v is field independent since it is a quantity associated with the single-vortex regime.

D. Diffusion of defects in the vortex lattice

Because of the fixed size of a VL interstitial (vacancy) and the fixed length scale for a thermally activated hop (namely, the flux-lattice spacing a_0), the activation energy for thermally activated motion is independent of driving force. The problem of VL interstitial motion then reduces to that of thermal diffusion of a "flux particle," such as described in Ref. 12. The diffusion coefficient equals the product of the flux-flow resistivity ρ_f ,² the interstitial concentration $n_v a_0^2$, and an activation term.

It is not clear *a priori* what form ρ_f should have. Namely, the viscosity associated with motion of a dislocation pair need not be that of a single vortex. Nevertheless, in our assumption that small pairs are most important, we shall use the expression for the flux-flow resistivity, $\rho_f = 1.1\rho_n B/B_{c2}$,³¹ for simplicity. The upper critical field B_{c2} has been calculated by Werthamer, Helfand, and Hohenberg.³²

In order to evaluate the activation barrier, we point out that VL interstitial motion is hindered by the pinning potential as well as the presence of the surrounding vortices. In general, a thermally activated jump of the interstitial means a redistribution of vortices in its vicinity, resulting in a redefinition of the interstitial's position a distance a_0 removed from its prior site. Modeling the deformation field caused by the interstitial as a solitonlike wave, the sum of displacements related with the redistribution can be shown to be of order a_0 . We account for this by taking the variance σ (over a distance a_0) of the random pin potential U_v (knowing that U_v is the variance associated with an interstitial displacement over a distance ξ):

$$\sigma = \langle (\delta U_v)^2 \rangle^{1/2} \approx U_v \left[\frac{a_0}{\xi} \right]^{1/2}. \quad (6)$$

Note that the factor $(a_0/\xi)^{1/2}$ also produces the only field dependence in the activation energy $\sigma \propto B^{-1/4}$. Combining Eqs. (5) and (6), we find the temperature dependence to be

$$\sigma \equiv \sigma(0) f(t) \propto B_c^2 \xi^{1/2} (1+t)^{-4} \\ = \sigma(0) (1+t)^{-2} (1-t)^{7/4}. \quad (7)$$

For the interstitial concentration we distinguish two regimes. In the low-temperature regime, the residual, pinning-induced VL dislocation pairs will be most important. Their concentration has been estimated as $n_v a_0^2 \approx \exp(-U_e^2/2\sigma^2)$ (Ref. 22) and as $n_v a_0^2 \approx \exp(-U_e/\sigma)$.²³ At higher temperatures thermally induced dislocation pairs will dominate, and $n_v a_0^2 \approx \exp(-U_e/k_B T)$.

Summarizing, we have, for the diffusion coefficient,

$$D_0 = \frac{\rho}{\mu_0} \approx \frac{\rho_f}{\mu_0} n_v a_0^2 \exp \left[-\frac{\sigma}{k_B T} \right], \quad (8)$$

where ρ is the resistivity caused by TAFF in a transport measurement. Note that the only free parameter in this expression is the oxygen vacancy concentration n_v , figuring in Eq. (5).

A comparison of the barrier for elastic creep [Eq. (1)] to U_e yields a crossover current density j_3 ,²² below which dislocation-mediated (plastic) flux creep is important. Comparing $U(j)$ to σ instead of U_e , the crossover criterion may be modified to describe the low-temperature case, from which it becomes

$$j \lesssim j_3 = j_c \left[\frac{R_c r_f^2}{a_0^3} \right]^{8/9} \left[\frac{r_f}{\alpha a_0} \right]^{4/9}. \quad (9)$$

R_c is the transverse characteristic dimension of a correlated region in the 2D vortex lattice. From recent VL decoration experiments by Murray *et al.*,³³ we have $R_c \approx 2 - 4a_0$.

E. TAFF model of flux diffusion

In this subsection the application of the thermally assisted flux-flow (linear flux diffusion) model to ac-susceptibility experiments is briefly reviewed. Because vortices can only be created at the sample surface, the induction in the bulk of the sample obeys the continuity equation $\partial B / \partial t = (\partial / \partial r) D_0 \partial B / \partial r$ (for a cylindrical sample). r is a coordinate along the sample radius; D_0 is the same quantity as in Eq. (8). Solving this in the case of a large constant field with a sinusoidal ripple of frequency ν at the sample boundary, $B = \mu_0 (H_0 + h_{ac} \cos 2\pi \nu t)$, yields an exponential flux profile, with decay length $\lambda_{ac} = (D_0 / \pi \nu)^{1/2}$. This length has been called the flux-flow skin depth, in analogy to the normal-state skin effect.³⁴

At low temperatures the diffusion coefficient becomes exponentially small. The main contribution to the permeability will then come from the ac response of the pinned VL.³⁵ The elastic displacement of the vortices from their equilibrium positions in their pinning potential wells results in a net ac-field penetration. This penetration, too, is exponential in the distance from the sample surface. The corresponding characteristic decay length $\lambda_c = (B^2 / \mu_0 \alpha_L)^{1/2}$ was called the pinning penetration depth,³⁵ where $\alpha_L = j_c B / r_f$ is the Labusch constant.

The two contributions to the permeability, elastic response and thermal activation, may be combined by adding the resulting vortex flow velocities: $v = v_{TA} + v_{el}$. The continuity equation is modified to

$$\dot{B} = \frac{\partial}{\partial r} \lambda_c^2 \frac{\partial \dot{B}}{\partial r} + \frac{\partial}{\partial r} D_0 \frac{\partial B}{\partial r}. \quad (10)$$

Solving this equation, the ac penetration depth is found to be $\lambda_{ac} = |k_+ + ik_-|^{-1} = (k_+^2 + k_-^2)^{-1/2}$, where

$$k_{\pm} = \frac{1}{\sqrt{2}} \left[\left(\frac{\omega^2}{D_0^2 + \omega^2 \lambda_c^4} \right)^{1/2} \pm \left(\frac{\omega^2 \lambda_c^2}{D_0^2 + \omega^2 \lambda_c^4} \right)^{1/2} \right]. \quad (11)$$

Here $\omega \equiv 2\pi\nu$. Because of the exponential form (8) of D_0 , there is only a narrow temperature range where both mechanisms contribute to the permeability to the same extent.

The onset of irreversible behavior occurs when λ_{ac} equals a/M_0 , where a is a characteristic sample dimension and M_0 a constant determined by sample geometry. For a cylinder this is the radius; for a slab it is half the thickness. The infinite slab was treated in Ref. 12 and the cylinder of infinite length in Ref. 34. There it was shown that the permeability

$$\mu \equiv 1 + \chi = \frac{2\lambda_{ac}}{ia} \frac{I_0'(a/\lambda_{ac})}{I_0(a/\lambda_{ac})}. \quad (12)$$

$I_0(x)$ is the zeroth-order modified Bessel function; the accent denotes the first derivative to the argument. The complex susceptibility is written as $\chi = \chi' + i\chi''$. The constant M_0 is defined by plotting the solution for the permeability^{12,34} versus a/λ_{ac} (Fig. 1) and choosing a criterion related to a well-defined experimental feature. Two convenient choices are the a/λ_{ac} value, where a linear extrapolation of the real component μ' intercepts $\mu = 1$, and the a/λ_{ac} value, where the imaginary component μ'' is maximum. Both features reveal the onset of irreversibility.⁴ The corresponding values of M_0 are 0.56 or 1.13 for the slab geometry and 1.25 or 2.57 for the cylindrical geometry.

At the irreversibility onset, we now have

$$\nu = \frac{M_0^2}{\pi a^2} D_0 = \frac{M_0^2}{\mu_0 \pi a^2} \rho \propto \rho_f n_v a_0^2 \exp \left[-\frac{\sigma}{k_B T} \right]. \quad (13)$$

Because D_0 is a function of B and T , Eq. (13) determines the irreversibility line of a HTS at the frequency ν . Consequently, the irreversibility line, denoted at $T_{irr}(B)$ or $B_{irr}(T)$, shifts with frequency.^{4,5}

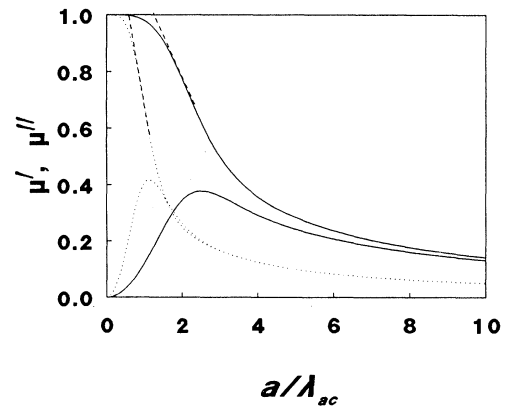


FIG. 1. Solutions of the ac permeability of an infinite slab (dotted lines) compared with that of a cylinder of infinite length (solid lines), as a function of the variable a/λ_{ac} (see text). The procedures for obtaining M_0 are illustrated by the extrapolation of the μ' curves to 1 as indicated by the dashed lines; in the case of μ'' , M_0 is the value of a/λ_{ac} that corresponds to the peak position.

ac-susceptibility and resistivity experiments share the condition that they are carried out at a low current density and thus probe the same type of flux creep. According to Eq. (8), the diffusion coefficient governing VL interstitial motion is essentially equal to the resistivity. Therefore, at a fixed applied dc field the frequency and temperature at which χ'' (or μ'') is maximum are related to each other in a manner analogous to the way the resistivity transition and temperature are related, namely, according to an Arrhenius expression.³ A plot of $\ln v$ versus T_{irr}^{-1} should thus yield the same information on the activation barrier as a plot of $\ln \rho$ versus T^{-1} . The choice of a resistance threshold defining the onset of irreversibility in a resistance measurement corresponds to a choice of the measurement frequency in an ac-susceptibility experiment.

III. RESULTS

A. ac-susceptibility experiment

The measurements of the complex susceptibility on the Bi-Sr-Ca-Cu-O single crystal ($T_c = 83$ K; dimensions, $1.0 \times 0.8 \times 0.2$ mm³), presented in Ref. 5, were extended to different applied dc fields. In all measurements the dc field was applied perpendicular to the (a, b) plane of the sample. The measurements were carried out using a standard mutual inductance technique. The primary coil was compensated with a concentric coil so as to achieve zero mutual inductance with the superconducting magnet. In addition, the entire coil system was firmly clamped to the superconducting magnet. The measurements were taken over a frequency range 10.87 Hz $< \nu < 22$ kHz, in dc fields between 0.0075 and 6 T. The amplitude of the ripple field $\mu_0 h_{\text{ac}}$ was 3×10^{-5} T. The measurements were started from a high temperature where the induction completely penetrates the sample, so that corrections to the applied-field value due to demagnetizing effects are expected to be negligible.

Results for $\nu = 21.75$ Hz at selected field values are

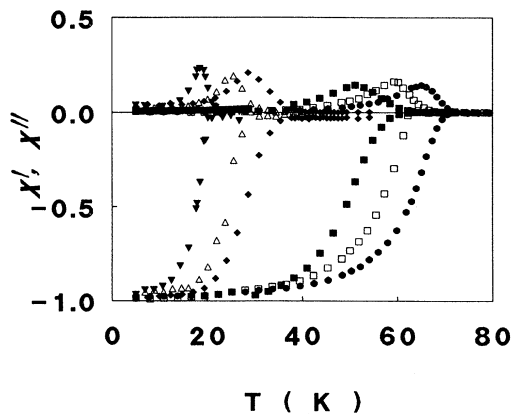


FIG. 2. Field dependence of the ac-susceptibility transition of the Bi-Sr-Ca-Cu-O single crystal for $\nu = 22$ Hz. The symbols represent the following applied dc-field values: solid triangles, 4 T; open triangles, 1 T; solid diamonds, 0.4 T; solid squares, 30 mT; open squares, 15 mT; solid circles, 7.5 mT.

shown in Fig. 2. The susceptibility transition is found to be strongly field dependent. The downward shift of the transition temperature with increasing fields is most pronounced at the lowest fields. Also, the width of the transition is greater at lower field values. The magnitude of both the inductive component χ' and the dissipative component χ'' is field dependent. The magnitude of χ' decreases somewhat, while that of χ'' is enhanced as the field is increased. The data were calibrated by dividing the signal by the signal in zero applied field at low temperature, $T = 4.2$ K.

Direct measurements of the permeability can in principle be performed by balancing the Meissner signal of the sample with a compensating coil. The signal observed in an applied field is then directly proportional to the ac-field penetration in the sample.³⁵ Variation of the ripple-field amplitude yields the flux profile. The magnitude of the pinning penetration depth λ_c was estimated to be about 5 μm .

Values of the irreversibility temperature T_{irr} were determined using the two criteria corresponding to the above choices for M_0 : the zero intercept T'_{irr} of a linear extrapolation of the χ' transition and the peak in χ'' , at $T = T''_{\text{irr}}$. Here the sample was approximated by a cylinder of radius 0.51 mm, corresponding to $\sqrt{A/\pi}$, with A the sample cross section perpendicular to the applied-field direction. A plot of B versus T_{irr} represents the irreversibility line.⁴ The results for $\nu = 87$ and 696 Hz are shown in Fig. 3.

Also in Fig. 3 are the temperatures where the dc magnetization of the same sample becomes unobservably small ($J \approx 10^6$ A/m²). This "dc"-irreversibility line looks very much like the lines obtained via ac susceptibility. The measured irreversibility lines also closely resemble ac-susceptibility and mechanical oscillator results obtained by Gammel³⁶ and results of ac- and dc-

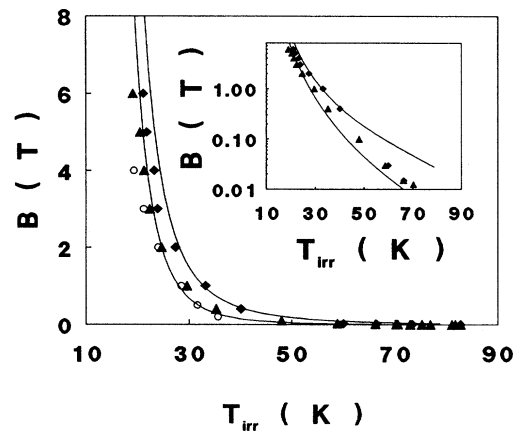


FIG. 3. Irreversibility lines for the Bi-Sr-Ca-Cu-O sample, with $\nu = 87$ Hz (triangles) and $\nu = 696$ Hz (diamonds). Open circles represent the field values where irreversible dc magnetization becomes unobservably small. Solid lines denote model fits, with $n_{\square} \approx 7 \times 10^{17}$ m⁻² (see Sec. III B 1). The inset shows the figure on a logarithmic scale, data obtained from the dc measurements having been omitted.

susceptibility by Gupta *et al.*^{6,37} and de Rango *et al.*³⁸

Decreasing the ripple-field amplitude by a small factor had no influence on the susceptibility transition. It can therefore be concluded that the measurements were indeed carried out in the TAFF regime, where the activation barrier is independent of driving force. An increase of the ripple-field amplitude by a factor of 10, however, yields the result illustrated in Fig. 4. The depicted curves were measured in a dc field of 1 T, at a frequency $\nu=21.75$ Hz. A slight dependence of T'_{irr} and T''_{irr} on driving-field amplitude is now observed. The low-temperature onset of the χ'' peak is shifted to a distinctively lower temperature. The broadness of the χ' transition is affected, the diamagnetic signal diminishing at a lower temperature when a larger amplitude is used. Details of the amplitude dependence will be presented elsewhere.

In Fig. 5, $D_0 = \pi\nu a^2 / M_0^2$ has been plotted logarithmically versus T_{irr}^{-1} , as obtained both from the in- and out-of-phase susceptibility. The values $M_0 = 1.13$ and 4 have been used for the two respective cases. The deviation from the values stated in Sec. II E is due to the irregular geometry of the sample. By plotting the irreversibility temperatures in this way, the data range can be increased from three to more than four decades. T'_{irr} and T''_{irr} scale approximately as the logarithm of the frequency of the ripple field. The plot of D_0 versus inverse temperature is very much similar to the resistivity results of Palstra *et al.*³ Our data correspond to a resistivity range between 8×10^{-5} and $4 \times 10^{-1} \mu\Omega \text{ cm}$. The linear scaling of $\ln\nu$ with T_{irr}^{-1} seems to break down at the lowest fields and frequencies. Measurements carried out in fields below 0.1 T show that below $\nu \approx 100$ Hz the apparent transition temperature is much less frequency dependent than above this frequency.

Because the main contribution to the diffusion coefficient D_0 comes from the exponential term, the slope of a linear fit to the T_{irr} data for a given field yields an estimate of the activation barrier at that field. These slopes are depicted in Fig. 6(a), along with data from Ref. 3.

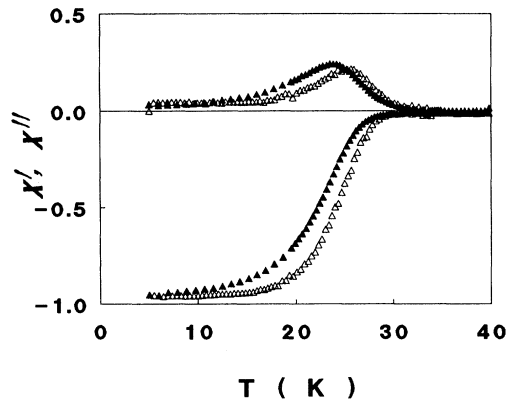


FIG. 4. Susceptibility transition of the Bi-Sr-Ca-Cu-O sample in an applied field of 1 T, at driving field amplitudes $\mu_0 h_{\text{ac}}$ of 0.03 (open triangles) and 0.3 mT (solid triangles), at a frequency of 22 Hz.

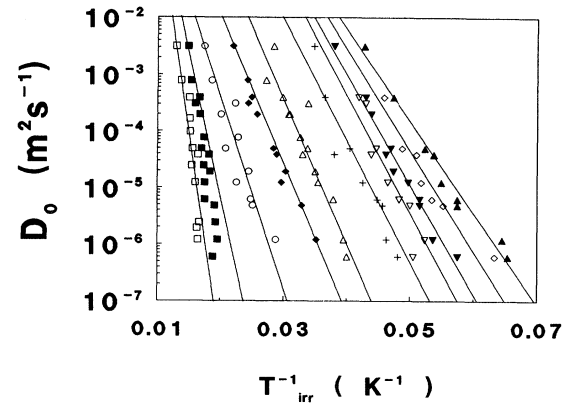


FIG. 5. Measured values of the diffusion coefficient D_0 as determined from linear extrapolation of the χ' transition to zero and from the peak positions of χ'' . The field dependence of the activation energy is derived indirectly from the straight lines through the data. The symbols denote the following applied-field values: solid triangles, 6 T; open diamonds, 5 T; solid inverted triangles, 4 T; open inverted triangles, 3 T; crosses, 2 T; open triangles, 1 T; solid diamonds, 0.4 T; circles, 0.1 T; solid squares, 30 mT; open squares, 15 mT.

The results are very similar to those obtained by Gammel³⁶ and also to recent results by Hsu and Kapitulnik on very thin Nb films.³⁹ Below a certain crossover field, here approximately 1 T, the slopes follow a power law $\sim B^{-1/6}$; above this field a power of $B^{-1/3}$ is observed. The behavior observed in Ref. 36 is in fact a power $B^{-0.14}$ below and $B^{-0.25}$ above the crossover field.

In order to obtain the true field dependence of the activation barrier, we should correct for the temperature dependence $f(t)$ given in Eq. (7). A graph of $f(t)$ versus t is shown in Fig. 6(b). The correction procedure followed was to plot $-f(t)/t$ as a function of t^{-1} . The slope of this curve was determined at the average reduced irreversibility temperatures \bar{T}_{irr} , for respective values of the magnetic field. Subsequently, the measured slopes were divided by these factors, which were from 1.37 at field values above 2 T to 3.26 for 15 mT. The resulting values $U(0)$, which should be considered as the *experimentally* determined zero-temperature magnitude of the activation barrier at different fields, are shown in a double-logarithmic plot in Fig. 6(c). The data obtained in Ref. 3 have been elaborated in the same way and are added to the figure. The activation energy decreases from approximately 500 K at $B=15$ mT to about 250 K at $B=7.5$ T. The data cannot be considered conclusive as to the precise functional behavior, although at fields above 1 T, it is close to a power law $B^{-1/4}$, indicated by the solid line. Below 1 T the field dependence is approximately $B^{-1/10}$.

B. Comparison of data with theory

The exponential decay of the flux profile in the sample at the lowest measuring temperatures allows us to esti-

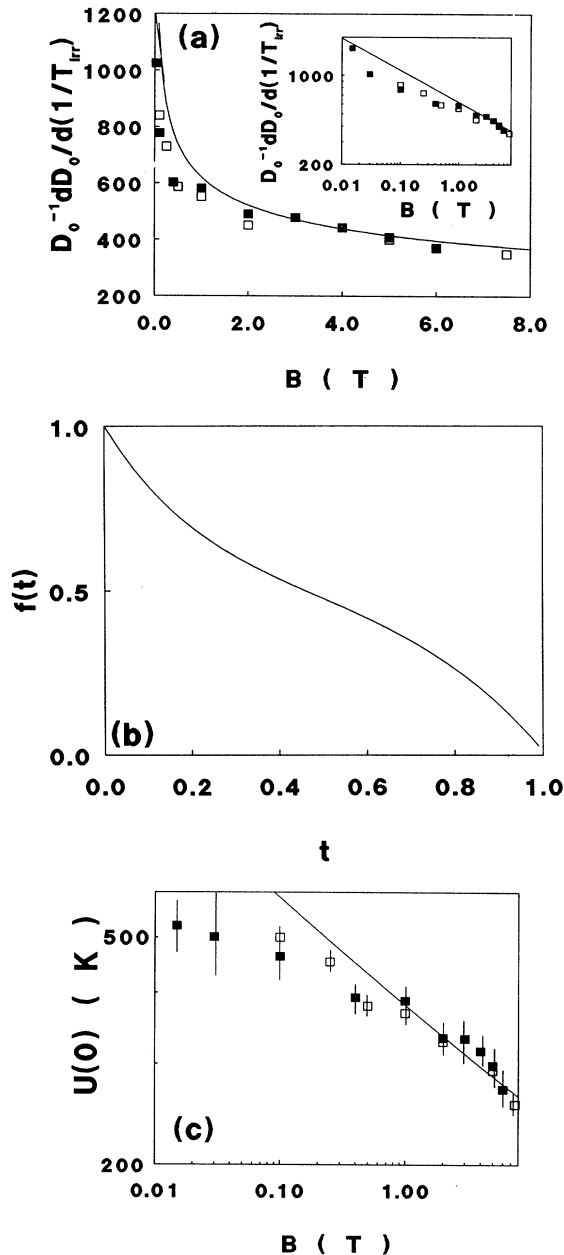


FIG. 6. (a) Field dependence of the slopes of the Arrhenius plots in Fig. 5, compared to the $B^{-1/4}$ dependence (solid line). Solid squares are data obtained from Fig. 5; open squares are data from a resistivity measurement by Palstra *et al.* (Ref. 3). The inset shows the figure on a double logarithmic scale. Low-field data ($B < 1$ T) show a $B^{-1/6}$ dependence; high-field data ($B > 1$ T) show a $B^{-1/3}$ dependence. The line follows $B^{-1/4}$. (b) Temperature dependence of the activation energy of a VL interstitial (6), as described in the text. Reduced units for $t \equiv T/T_c$ and $f(t) \equiv \sigma(T)/\sigma(0)$ are used for the abscissa and ordinate, respectively. (c) $U(0)$ vs B obtained following the correction procedure outlined in Sec. III A. Symbols refer to the same data as in (a). The drawn line is a fit of the high-field data to $U_e + \sigma$, as described in the text. Lines through the data points reflect the inaccuracy in the determination of the activation energy.

mate the maximum current density resulting from the ripple field h_{ac} , $j = \partial h_{ac} / \partial r \approx h_{ac} / \lambda_c$. Knowing the ripple-field amplitude $\mu_0 h_{ac} = 3 \times 10^{-5}$ T and the pinning penetration depth $\lambda_c \approx 5 \mu\text{m}$, we arrive at a value of the order $5 \times 10^5 \text{ A m}^{-2}$. This is more than three orders of magnitude lower than the value of j_c we shall obtain below, so that a considerable enhancement of $U(j)$ is expected, to such an extent that the condition (9) may be satisfied. We thus expect the plastic-flux-creep model to apply.

1. Irreversibility line

Using Eq. (8) for the diffusion coefficient, the flux-flow penetration depth $\lambda_{ac} = (k_+^2 + k_-^2)^{-1/2}$ may be calculated by means of Eq. (11), with $\lambda_c = 5 \mu\text{m}$ and $\nu \equiv \omega/2\pi$ the measuring frequency. The flux diffusion coefficient was evaluated using the normal-state resistivity $\rho_n \approx 50 \mu\Omega \text{ cm}$, the expressions (5) and (6), and the various forms for the VL interstitial concentration $n_v a_0^2$ mentioned in Sec. II D. For $\xi(0)$ and $\lambda(0)$, the values 2.3 and 290 nm were taken. The irreversibility line is now found by equating λ_{ac} to a/M_0 . The theoretical values $M_0 = 1.25$ and 2.57 have been used, corresponding to the infinite circular cylinder. A fit to the experimental data in Fig. 3 yields n_\square , the areal density of oxygen vacancies per CuO_2 double layer.

Satisfactory fits could be made only using the thermal-activated form

$$n_v a_0^2 \approx \exp \left[- \frac{U_e}{k_B T} \right]. \quad (14)$$

The fits of the irreversibility lines obtained from χ' for $\nu = 87$ and 696 Hz are shown in Fig. 3. The inset shows the same figure on a semilogarithmic scale. The parameter n_\square turned out to be $3.5 \times 10^{17} \text{ m}^{-2}$. Similar results have been obtained for $T''_{irr}(B)$. The resulting value for $\sigma(0)$ is 160 K at $B = 1$ T. Surprisingly, the theory of 2D plastic flux creep describes the irreversibility line reasonably well to low fields where the sample is expected to show more 3D-like behavior.

We have also attempted to fit the data using the two expressions estimating the disorder-induced VL dislocation density. The form $n_v a_0^2 \approx \exp(-U_e/2\sigma^2)$ yielded a decreasing diamagnetic onset temperature with increasing pinning strength, an unphysical result. The expression $n_v a_0^2 \approx \exp(-U_e/\sigma)$ results in a low-temperature dislocation density of about 50%. This is in contradiction with the observation in the flux decoration experiment by Murray *et al.*³³ that the total dislocation concentration amounts to only a few percent.

The value $n_\square = 3.5 \times 10^{17} \text{ m}^{-2}$ means that 1 in every 80 oxygen atoms is missing in each CuO_2 single layer, which seems a reasonable fraction. Since the dimension of the vortex core is typically $\pi \xi^2 = 2.3 \times 10^{-17} \text{ m}^2$, there are about 8 active pinning centers interacting with each 2D vortex. The interaction of the pins with the vortex core is therefore collective. The parameter α is evaluated at ≈ 0.5 . This means that vortices are pinned almost independently and that R_c is very small.

2. Activation barrier

When looking at the field dependence of the activation barrier [Fig. 6(c)], it is clear that data sets obtained through resistivity and ac susceptibility compare favorably, indicating that the same mechanism determines the resistive and ac-susceptibility transition. This conclusion was drawn for $\text{YBa}_2\text{Cu}_3\text{O}_{7-\delta}$ in Ref. 40. The increase at low fields is in qualitative agreement with theoretical expectation, but the $B^{-1/4}$ dependence is only approached at fields above $B=1$ T. The drawn line in Fig. 6(c) represents a calculation of the VL interstitial energy $U_e + \sigma(T, B)$. Here the same values of $\xi(0)$ and $\lambda(0)$ as above have been used. Because the temperature dependence of U_e in the relevant temperature regime is weak, we have ignored its effect on the correction procedure outlined in Sec. III A. It is, however, necessary to invoke the presence of U_e in the activation term [Eq. (14)] in order to explain the measured magnitude of the energy barrier $U(0)$. The exact magnitude of $U(0)$ in Fig. 6(c) was reproduced taking n_{\square} as $0.6 \times 10^{18} \text{ m}^{-2}$, slightly larger than the value obtained from the fit of the irreversibility line in Fig. 3. The difference is not too surprising in view of the remaining uncertainty in the value of the penetration depth λ : both U_e and σ depend inversely quadratically on this quantity.

3. Susceptibility curves

From λ_{ac} we may also calculate the actual shape of the ac-susceptibility transition. From Eq. (12), with $\nu=696$ Hz and the same parameter values as in Sec. III B 1, the curves in Fig. 7 are obtained. Here the χ'' data have been multiplied by factors between 1.29 (for $B=4$ T) and 2 (for $B=0.1$ T) so as to scale them to the magnitude of the calculated curves. The shapes of the χ' curves and the field dependence of the diamagnetic onset temperature are well reproduced. When comparing the χ'' curves, we find that the peak positions and low-temperature sides are well reproduced, but the high-temperature sides deviate significantly from the calculated curves. The data points then lie systematically below the calculated curves.

IV. DISCUSSION

From the value $n_{\square}=3.5 \times 10^{17} \text{ m}^{-2}$ obtained by fitting the experimental data, the pinning force density can be evaluated. Substitution of n_{\square} yields the net pinning force per vortex, $F_v \approx 2 \times 10^{-13}$ N, and the pinning energy $U_v = 5 \times 10^{-22}$ J ≈ 35 K. The critical current density at zero temperature follows from $j_c = F_v / \Phi_0 d$ and is estimated to be $5 \times 10^{10} \text{ A m}^{-2}$. This value is about an order of magnitude larger than the current density as calculated from magnetization hysteresis loops, measured in the same sample by van den Berg *et al.*⁵ An explanation for the large difference is provided by the modest value of the pinning energy, which allows very fast decay of the flux profile after and during changes of the applied field. The measured magnetization value does not correspond to the critical current but to a much lower shielding current. After long times, or at high temperatures and

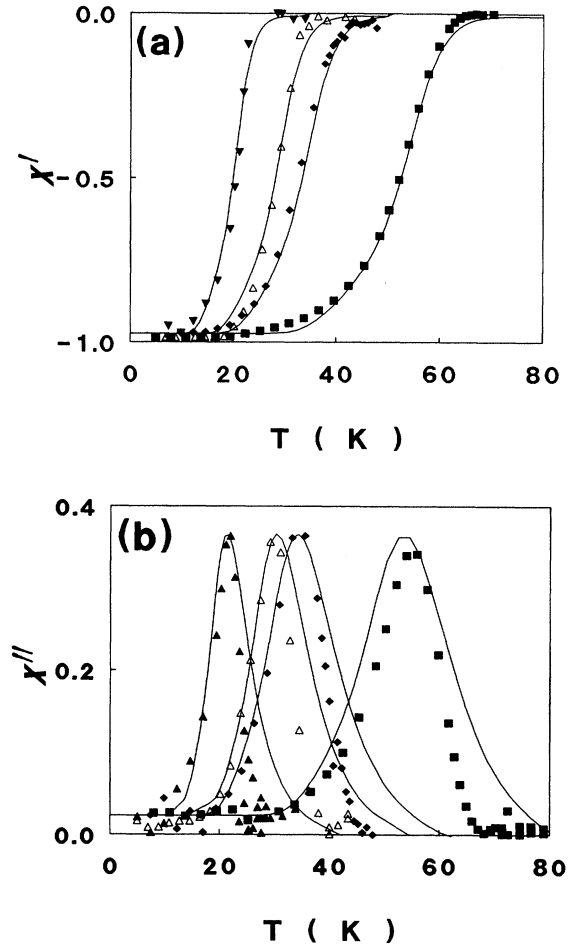


FIG. 7. Fit (solid lines) of the plastic-flux-creep model to the susceptibility transition of the Bi-Sr-Ca-Cu-O single crystal at a frequency of 696 Hz. Symbols denote the same field values as in Fig. 2. The value of n_{\square} was the same as taken for the fit in Fig. 3.

fields, the current decreases below $j_3 \approx 5 \times 10^8 \text{ A m}^{-2}$, below which plastic flux creep is expected to prevail. The temperature where the irreversibility of the dc magnetization becomes unobservably small should therefore be described by plastic creep.

These irreversibility temperatures have been extracted from the results in Ref. 5 and are included in Fig. 3. The temperature values depend on such parameters as the lowest observable current density J_{\min} , sweep rate of the magnetic field \dot{H} , and sample radius a . The value of J_{\min} was $1 \times 10^6 \text{ A m}^{-2}$. From TAFF we can in principle predict the dc-irreversibility line for a cylinder using the criterion given in Ref. 12:

$$D_0 = \frac{3\dot{H}a}{8J_{\min}}. \quad (15)$$

The sweep rate of the dc field was $\mu_0\dot{H} = 2.5 \times 10^{-3}$ T/s. The irreversibility lines obtained from dc magnetization and ac susceptibility with $\nu=87$ Hz are almost identical. Evaluating the “irreversibility condition” for

the latter, we find $D_0 \approx 4.4 \times 10^{-5} \text{ m}^2 \text{ s}^{-1}$ [using Eq. (13)]. By inserting J_{\min} in Eq. (15), however, the condition $D_0 \approx 3.8 \times 10^{-7} \text{ m}^2 \text{ s}^{-1}$ is obtained. The large difference can be understood if one considers the crude determination of the irreversibility temperatures. An error of 20% is sufficient to explain the discrepancy in the value of the diffusion coefficient. Also, the irregular sample geometry may account for part of the error. Multiplying the right-hand side of Eq. (15) with an appropriate constant, the same irreversibility line as for $\nu = 87 \text{ Hz}$ may be recovered (Fig. 3). This means that the onset of irreversible magnetic behavior can be at least qualitatively described by plastic creep. It was shown in Ref. 1 that the decay rates of magnetization and measured current densities in a field-sweep experiment are mutually consistent within the TAFF model.

The importance of pinning in Bi-Sr-Ca-Cu-O was recently illustrated in measurements of the dc magnetization on Bi-Sr-Ca-Cu-O carried out by Kritschna *et al.*⁴¹ The measurements were performed on a single-crystalline Bi-Sr-Ca-Cu-O sample prior to and following exposure to fast neutrons. The irreversibility line was found to shift to higher temperatures following the irradiation. This can be interpreted as a consequence of the enhanced pinning caused by the introduction of crystal-lattice defects. A model describing the onset of irreversibility should therefore account for a dependence on the pinning strength. It must be noted, however, that the pinning structures resulting from neutron-irradiation damage are typically extended defects, or clusters of defects, in contrast to the above description in terms of point defects.

The observed dependence of the susceptibility transition on driving-field amplitude h_{ac} can be explained by the criterion [Eq. (9)] describing the crossover between the regions of plastic versus elastic flux creep. The driving-field amplitude enters this expression through the current j . Substituting

$$j = \partial h_{ac} / \partial r \approx (h_{ac} / \lambda_{ac}) \exp(-r / \lambda_{ac}),$$

it can be readily seen that plastic creep will be important when $h_{ac} / \lambda_{ac} < j_3 \approx j_c (\xi / a_0)^2$. Substitution of the parameters yields $\mu_0 h_{ac} / \lambda_{ac} < 250B \text{ (T/m)}$. Thus, when the driving-field amplitude is increased, the left-hand side becomes larger, indicating a more important contribution of elastic creep to flux transfer. This is in agreement with the experiment, where dissipation (χ'') is enhanced and the diamagnetic transition (χ') smeared out when h_{ac} is increased (Fig. 4). The deviation is more pronounced at lower dc fields, in agreement with theory.

An alternative explanation of the h_{ac} dependence of the transition is provided by taking into account the effect of the equilibrium (Abrikosov) flux density. For the case of a field-cooled experiment on a high- κ superconductor, it was shown very recently that this results in a remanent flux profile, corresponding to a temperature-dependent flux-trapping depth.⁴² Applying a larger ripple-field amplitude can release the vortices from the trapped configuration, thus bringing the sample into a more homogeneous state. The nature of the h_{ac} dependence is currently under study.

Returning to the criterion [Eq. (9)], it can be seen that since the ac penetration depth increases with temperature (through its dependence on D_0), elastic creep should be most relevant at low temperatures. In the low-temperature regime plastic flux creep is negligible because the diffusion coefficient is exponentially small. The low-energy barrier U_c associated with elastic creep in the critical state²² can then explain the rapid decay with time of nonequilibrium magnetization. Furthermore, the decay of low-temperature magnetization is nonexponential,⁴³ in contradiction to the prediction of TAFF.

Finally, elastic creep should become more important at lower dc fields, where the activation barrier for plastic flux creep increases rapidly. The low-field region is indeed that where the χ'' components deviate most from plastic creep theory. However, it may also be that the magnetic coupling between vortex disks in adjacent CuO_2 double layers becomes important enough to yield a more three-dimensional VL. The change in field dependence of the activation energy may well be an indication of this. It is noteworthy that the slopes of Arrhenius plots of the resistivity of the ultra-thin Nb films presented in Ref. 39, for which 2D behavior is clearly expected, only exhibited a power-law dependence as $B^{-1/3}$. This corresponds to the field region $B > 1 \text{ T}$ in Fig. 6(a). Identifying the change in field dependence with the expected dimensional crossover in Bi-Sr-Ca-Cu-O (Sec. II A), we have $B_{2D} \approx 1 \text{ T}$. This agrees quite well with theoretical predictions of 0.3 T (Ref. 22) and 3 T.²³

The fact that the VL dislocation density is well described by the thermally activated form [Eq. (14)] over the entire experimentally accessed temperature range indicates that the greater part of the (T, B) phase diagram of the VL in Bi-Sr-Ca-Cu-O, e.g., for $T > 15 \text{ K}$, can be considered a "high-temperature" regime. This means that above 15 K the vortex glass state is destroyed by VL dislocations. Evaluating the temperature where $n_v a_0^2 = 0.5$, a value of 70 K is found. The vortex lattice may thus be expected to be melted over a broad temperature range below T_c . The onset of such a dislocation-mediated melting transition⁴⁴ is reflected in the renormalization of the shear modulus. The core energy of dislocations will then drop. This process may explain the deviation from theory of the high-temperature side of the χ'' curves, a steeper descent, indicating a larger mobility of vortices.

V. CONCLUSION

In summary, we have found that the ac-susceptibility transition in Bi-Sr-Ca-Cu-O is well described by the diffusion of interstitials and vacancies in the vortex lattice. Diffusion of a VL dislocation is analogous to that of a particle and is described by the TAFF model. The activation barrier for thermally assisted flux flow is independent of driving force and consists of two parts: the elastic energy $U_e \approx 100 \text{ K}$, determined by the shear modulus c_{66} , and the variance over a distance a_0 of the pinning energy, $\sigma \approx 160 \text{ K}$ (at $B = 1 \text{ T}$). The latter energy depends on the square root of the concentration of pinning centers and scales approximately as $B^{-1/4}$. Consid-

ering pinning to be caused by oxygen vacancies in the CuO_2 double layers, we find an areal density of oxygen vacancies of $3.5 \times 10^{17} \text{ m}^{-2}$, one per eight formula units. Deviations from the theory of plastic flux creep can be explained by assuming a creep contribution from elastically correlated regions in the VL. This becomes particularly manifest at fields $B < B_{2D} \approx 1 \text{ T}$, when 2D vortex disks couple to vortices in adjacent superconducting layers. Above this field the VL may be melted over a large part of the (T, B) phase diagram.

ACKNOWLEDGMENTS

We thank M. Essers for her competent assistance, M. Menken for preparation of the Bi-Sr-Ca-Cu-O sample, Dr. V. M. Vinokur for the many helpful and stimulating discussions, and Dr. J. A. Mydosh and Dr. G. J. Nieuwenhuys for critically reading the manuscript. This work was supported in part by the Netherlands Foundation for the Fundamental Research on Matter (FOM).

*Also at ERDC, Los Alamos National Laboratory, Los Alamos, NM 87545.

- ¹J. van den Berg, C. J. van der Beek, P. Koorevaar, P. H. Kes, J. A. Mydosh, M. J. V. Menken, and A. A. Menovsky, *Physica C* **162-164**, 1189 (1989).
- ²P. Berghuis, P. H. Kes, B. Dam, G. M. Stollman, and J. van Bentum, *Physica C* **167**, 348 (1990).
- ³T. T. M. Palstra, B. Batlogg, L. F. Schneemeyer, R. B. van Dover, and J. V. Waszczak, *Phys. Rev. B* **38**, 5102 (1988).
- ⁴A. P. Malozemoff, T. K. Worthington, Y. Yeshurun, F. Holtzberg, and P. H. Kes, *Phys. Rev. B* **38**, 7203 (1988).
- ⁵J. van den Berg, C. J. van der Beek, P. H. Kes, J. A. Mydosh, M. J. V. Menken, and A. A. Menovsky, *Supercond. Sci. Technol.* **1**, 249 (1989).
- ⁶A. Gupta, P. Esquinazi, H. F. Braun, and H. W. Neumüller, *Europhys. Lett.* **10**, 663 (1989).
- ⁷D. R. Nelson, *Phys. Rev. Lett.* **60**, 1973 (1988).
- ⁸E. H. Brandt, *Phys. Rev. Lett.* **64**, 1106 (1989).
- ⁹R. S. Markiewicz, *J. Phys. C* **21**, 1173 (1988).
- ¹⁰A. Houghton, R. A. Pelcovits, and A. Sudbø, *Phys. Rev. B* **40**, 6763 (1989).
- ¹¹M. P. A. Fischer, *Phys. Rev. Lett.* **62**, 1415 (1989).
- ¹²P. H. Kes, J. van den Berg, C. J. van der Beek, and J. A. Mydosh, *Supercond. Sci. Technol.* **1**, 242 (1989).
- ¹³V. M. Vinokur, M. V. Feigel'man, V. B. Geshkenbein, and A. I. Larkin, *Phys. Rev. Lett.* **65**, 259 (1990).
- ¹⁴A. I. Larkin and Yu. N. Ovchinnikov, *J. Low Temp. Phys.* **21**, 409 (1979).
- ¹⁵M. V. Feigel'man, V. B. Geshkenbein, A. I. Larkin, and V. M. Vinokur, *Phys. Rev. Lett.* **63**, 2303 (1989).
- ¹⁶M. Tashiki and S. Takahashi, *Solid State Commun.* **70**, 291 (1989).
- ¹⁷M. Murakami, M. Morita, K. Doi, and K. Miyamoto, *Jpn. J. Appl. Phys.* **28**, 1189 (1989).
- ¹⁸R. Wördenweber, P. H. Kes, and C. C. Tsuei, *Phys. Rev. B* **33**, 3172 (1986).
- ¹⁹P. H. Kes and R. Wördenweber, *Phys. Rev. B* **34**, 494 (1986).
- ²⁰H. J. Jensen, A. Brass, Y. Brechet, and A. J. Berlinsky, *Phys. Rev. B* **38**, 9235 (1988).
- ²¹D. E. Farrell, S. Bonham, J. Foster, Y. C. Chang, P. Z. Jiang, K. G. Vandervoort, D. J. Lam, and V. G. Kogan, *Phys. Rev. Lett.* **63**, 782 (1989).
- ²²V. M. Vinokur, P. H. Kes, and K. V. Koshelev, *Physica C* **168**, 29 (1990).
- ²³M. V. Feigel'man, V. B. Geshkenbein, and A. I. Larkin, *Physica C* **167**, 117 (1990).
- ²⁴M. P. A. Fischer, D. S. Fischer, and D. A. Huse, *Phys. Rev. B* **43**, 130 (1991).
- ²⁵P. H. Kes, J. Aarts, V. M. Vinokur, and C. J. van der Beek, *Phys. Rev. Lett.* **64**, 1063 (1990).
- ²⁶L. N. Bulaevskii, V. L. Ginzburg, and A. A. Sobyenin, *Physica C* **152**, 378 (1988).
- ²⁷S. Mitra, J. H. Cho, W. C. Lee, D. C. Johnston, and V. G. Kogan, *Phys. Rev. B* **40**, 2674 (1989).
- ²⁸J. R. Thompson, D. K. Christen, Y. R. Sun, B. C. Chakoumakos, B. C. Sales, H. R. Kerchner, J. G. Ossandon, and E. Sonder, *Physica B* **165/166**, 1453 (1990).
- ²⁹E. H. Brandt, *Phys. Rev. Lett.* **57**, 1347 (1986).
- ³⁰E. V. Thuneberg, J. Kurkijärvi, and D. Rainer, *Phys. Rev. B* **29**, 3913 (1984); see also E. V. Thuneberg, *Cryogenics* **29**, 236 (1989).
- ³¹J. Bardeen and M. J. Stephen, *Phys. Rev.* **140**, A1197 (1965).
- ³²N. R. Werthamer, E. Helfand, and P. C. Hohenberg, *Phys. Rev.* **147**, 195 (1966).
- ³³C. A. Murray, P. L. Gammel, D. J. Bishop, D. B. Mitzi, and A. Kapitulnik, *Phys. Rev. Lett.* **19**, 2312 (1990).
- ³⁴J. R. Clem, H. R. Kercher, and T. S. Sekula, *Phys. Rev. B* **14**, 1893 (1976).
- ³⁵A. M. Campbell, *J. Phys. C* **2**, 1492 (1969).
- ³⁶P. L. Gammel, *J. Appl. Phys.* **67**, 4676 (1990).
- ³⁷A. Gupta, R. Esquinazi, H. F. Braun, and H. W. Neumüller, *Phys. Rev. Lett.* **63**, 1869 (1989).
- ³⁸P. de Rango, B. Giordanengo, R. Tournier, A. Sulpice, J. Chaussy, G. Deutscher, J. L. Genicon, P. Lejay, R. Retoux, and B. Raveau, *J. Phys. (Paris)* **50**, 2857 (1989).
- ³⁹J. W. P. Hsu and A. Kapitulnik, *Appl. Phys. Lett.* **57**, 1061 (1990).
- ⁴⁰T. K. Worthington, F. H. Holtzberg, and C. A. Field, *Cryogenics* **30**, 417 (1990).
- ⁴¹W. Kritschna, F. M. Sauerzopf, H. W. Weber, G. W. Crabtree, Y. C. Chang, and P. Z. Jiang, *Europhys. Lett.* **12**, 179 (1990).
- ⁴²L. Krusin-Elbaum, A. P. Malozemoff, D. C. Cronmeyer, F. Holtzberg, J. R. Clem, and Zhidong Hao, *J. Appl. Phys.* **67**, 4670 (1990).
- ⁴³D. Shi and M. Xu (unpublished).
- ⁴⁴D. S. Fisher, *Phys. Rev. B* **22**, 1190 (1980).